CMPS: CONSTRAINED MIXED PRECISION SEARCH FOR POST-TRAINING QUANTIZATION

Anonymous authors
Paper under double-blind review

ABSTRACT

The increasing complexity of deep neural networks (DNNs) requires effective model compression to reduce their computational and memory footprints for deployment on resource-constrained hardware. Mixed-precision search is a prominent bit allocation method based on neural architecture search (NAS) that has been shown to significantly reduce the DNN footprint while preserving the accuracy of the model by allocating bits to each layers based on their quantization sensitivity. However, mixed-precision search is often defined as a dual optimization problem handled with a single heuristic objective function, which does not provide strong guarantees of the resulting compression rate. We propose a post-training reformulation of mixed precision search as an explicit constrained optimization problem, solved using interior-point methods within a framework based on NAS. Our method requires minimal calibration data, as few as 128 samples, in a post-training setting. We corroborate this approach with experiments that span multiple transformer architectures with up to 4 billion parameters, using the MXFP family of data formats. We show that this constrained formulation provides users with higher resolution over compression rates, and we show that explicitly satisfying hardware budgets while optimizing for accuracy can outperform uniform allocation methods, improving performance by up to several standard deviations over the uniform baselines.

1 INTRODUCTION

The development of efficient Deep Neural Network (DNN) deployment strategies for resource-constrained hardware has led to significant advancements in reduced-precision numerical formats. Researchers and industry consortia have proposed a variety of these formats, including established integer types (e.g., INT8/4), custom floating-point representations (e.g., FP8/6), and block-level schemes such as Block Floating Point (BFP), alongside the more recent Microscaling (MX) family, which encompasses MXFP and MXINT Jacob et al. (2018); Micikevicius et al. (2022); Drumond et al. (2018); Darvish Rouhani et al. (2023); Rouhani et al. (2023). These formats improve arithmetic density and energy efficiency, frequently by amortizing exponent costs across blocks of data. The adoption of low-precision data formats in modern accelerators, such as AMD's Instinct and Google's TPUs, highlights their importance for high-performance inference and training MLCommons (a;b).

Despite progress in format design, a persistent challenge is that DNN exhibits distinct and varied sensitivities to reduced precision and sparsity layer-wise and column-wise (Zhang et al. (2022a); Lee et al. (2024); Dettmers et al. (2022)). This heterogeneity means that uniformly applying a single numerical format across all layers often results in suboptimal trade-offs between model accuracy and computational efficiency. Current post-training quantization approaches for mixed-precision often address this by employing heuristics, such as layer-sensitivity metrics, to guide the allocation of different formats. While very successful and beneficial for their post-training nature—aligning with the established wisdom that training a full-precision model first and then compressing often yields superior results Li et al. (2020)—these heuristic-driven allocations often prefer custom weight encodings over exploiting hardware-provided data formats, leading to compression and decompression steps of weights during inference.

In contrast, Differentiable Neural Architecture Search (DNAS) offers a more principled path, by learning the optimal layer-wise (or block-wise) assignment of hardware-provided low precision data

formats through optimization Wu et al. (2018; 2019); Cai & Vasconcelos (2020; 2021). Historically, DNAS for mixed-precision operated in a training-aware setting. While successfully demonstrating learned allocation, these methods typically handled hardware constraints by incorporating them as soft penalties within a multi-objective loss function. This often requires significant hyperparameter tuning and extensive exploration of the Pareto front to find a desirable balance between accuracy and model size, as the trade-off is not explicitly controlled.

This work seeks to bridge the advantages of both paradigms: the practicality and controllability of post-training methods with the optimized, learned allocation scheme of DNAS that can directly exploit the data formats provided by the deployment device. We revisit the challenge of hardware constraint integration for precision allocation, moving beyond soft penalties. We reformulate the problem within a DNAS-inspired post-training framework, treating hardware requirements as explicit, hard constraints. Our approach directly integrates model complexity into the optimization objective using a barrier-based interior-point method Boyd & Vandenberghen (2004); Nocedal & Wright (2006), systematically driving solutions towards feasibility while enabling fine-grained control over the final model complexity. This allows for a learnable, yet rigorously constrained, bit allocation in a post-training setting.

Our framework targets the post-training setting, using frozen weights and only a small calibration dataset. It operates on relaxed softmax-distributed architectural parameters and employs an annealed regularization schedule to efficiently solve the constrained optimization problem. This yields format allocations closely adhering to resource budgets while optimizing performance. Notably, our approach offers finer resolution in compression ratios and predictable model behavior across resource settings without retraining or finetuning. Our contributions are as follows:

- We introduce a novel, principled interior-point optimization framework for post-training, hardware-constrained bit allocation. This DNAS-inspired approach requires no model retraining or fine-tuning and operates effectively with as few as 128 calibration samples.
- Our framework provides fine-grained control over model compression, enabling stable and predictable performance across a higher resolution of intermediate compression ratios than typically available with fixed hardware format choices, bridging performance gaps.
- We demonstrate that our method enables smart, layer-wise precision allocation that goes beyond uniform quantization. This results in significant performance gains; for instance, with an average of only 4.5 effective bits, we achieve perplexity reductions of up to 9.06 points on C4 (Qwen2.5-1.5B) in few-shot settings and accuracy improvements of up to +10.7% (Qwen2.5-0.5B) in zero-shot evaluations compared to 4.25-bit uniform MXFP4 on the OpenAI Lambada benchmark.
- Crucially, our approach even allows models to outperform higher-precision uniform baselines using fewer bits. For example, our 4.5-bit mixed-precision Gemma models surpass both 6.25-bit and 8.25-bit uniform MXFP allocations on C4 perplexity and WikiText perplexity, showcasing substantial memory gains without sacrificing, and sometimes even improving, performance.

2 Related work

Low precision data formats The imperative to reduce the computational and memory footprint of Deep Neural Networks (DNNs) has spurred significant advancements in low-precision data representations. This area has seen a progression from conventional fixed-point integers (e.g., INT8, INT4) and custom floating-point types (e.g., FP8, FP6) towards more sophisticated block-based numerical formats (Jacob et al. (2018); Micikevicius et al. (2022); Gholami et al. (2021)). Block-based formats, which group multiple elements under a shared exponent or scaling factor, are particularly prominent as they improve arithmetic density while preserving essential dynamic range. For example, Drumond et al. (2018) proposed Hybrid Block Floating Point (HBFP), a representation where dot product operations utilize block floating point arithmetic, while element-wise functions and control logic retain the standard floating point. They showed that this hybrid strategy ensures comparable convergence to full-precision training (FP32) across various workloads and can achieve significant throughput gains with modest hardware modifications, positioning HBFP as a viable drop-in replacement.

More recently, Darvish Rouhani et al. (2023); Rouhani et al. (2023) developed the Microscaling (MX) data format family to support both inference and training. The MX formats combine narrow data types (e.g., INT8, FP6, FP4) with fine-grained block-level scaling. The authors designed these formats for high-performance computing environments, providing a tunable balance between computational efficiency, numerical stability, and usability. Their evaluations demonstrate that MX formats maintain model fidelity even for large-scale transformers using 8-bit and lower representations for activations, weights, and gradients. Furthermore, they show compatibility with common training pipelines and minimal need for hyperparameter or infrastructure adjustments. Consequently, MX formats are receiving considerable attention and support in next-generation hardware architectures (Open Compute Project (2023); Samson et al. (2024)).

Differentiable Neural Architecture Search The optimal bit allocation problem for neural networks is the following: Let a generic neural network of L layers labeled $l \in \mathbb{L} = \{1, ..., L\}$ with associated weight tensors $W = \{W^l\}_{l=1}^{L}$. Assuming we have access to a set of quantization functions labelled $Q_d(.)$ with $d \in \mathbb{D} = \{1, ..., D\}$, we define:

$$\begin{aligned} \hat{W}^l &\overset{def}{=} \sum_{d}^{D} A_d^l Q_d(W^l) \\ s.t. \quad & \sum_{d=1}^{D} A_d^l = 1 \quad \forall l \in \mathbb{L} \\ & A_d^l \in \{0, 1\} \quad \forall (l, d) \in \mathbb{L} \times \mathbb{D} \end{aligned} \tag{1}$$

Equation (1) represents the core formulation used in differentiable mixed-precision search frameworks. Wu et al. (2018); Cai & Vasconcelos (2020; 2021); Wu et al. (2019); Clark et al. (2018) aim to find the optimal decision variables A_d^l solving the multi-objective minimization problem:

$$\begin{aligned} \min_{\hat{W}, A} \quad & \mathcal{L}(A, \hat{W}) \\ \min_{A} \quad & \mathcal{C}(A) \end{aligned} \tag{2}$$

Here, $\mathcal{L}(A, \hat{W})$ is the model loss function, and $\mathcal{C}(A)$ is defined as a complexity cost on the architecture A, often related to hardware constraints such as size or latency. Throughout this paper, we set $\mathcal{C}(A)$ as the average bit width per element of the target model. The exponential number of possibilities for a choice of A and the latency induced by the evaluation of $\mathcal{L}$ make it difficult to efficiently solve the problem using combinatorial techniques. Taking inspiration from approximation algorithms, a popular approach is to relax the conditions on A and reinterpet A^l as a probability distribution.

$$\begin{cases} \sum_{d=1}^{D} A_d^l = 1 \\ A_d^l \in \{0, 1\} \end{cases} \implies \begin{cases} \sum_{d=1}^{D} A_d^l = 1 & \forall l \in \mathbb{L} \\ A_d^l \geq 0 & \forall (l, d) \in \mathbb{L} \times \mathbb{D} \end{cases} \tag{3}$$

To that end, Neural Architecture Search frameworks introduced the following parameterization of A^l in terms of logits $\{x^l\}_{l=1}^{L} \subset \mathbb{R}^D$:

$$A_d^l \equiv A_d^l(x^l) = \frac{exp(x_d^l)}{\sum_{k=1}^{D} exp(x_k^l)} \tag{4}$$

NAS-inspired frameworks for mixed precision quantization leverage the above relaxation by building a super-network, for which they train the weights and architectural parameters alternatively, handling the search for two sets of parameters at once. Once done, a feasible solution $\bar{A}$ to the original decision problem is rounded from the learned solution A to the relaxation by sampling each layer's bit-width from the learned distribution A^l. Cai & Vasconcelos (2021) propose to instead

select, for each layer, the quantization option with maximum probability, where the data format with the largest associated parameter is sampled. Wu et al. (2019); Wan et al. (2020) also propose the use of the Gumbel-Softmax to simulate random categorical sampling steps during the search phase and enforce the convergence of the distribution by scheduling the "temperature" hyperparameter of the Gumbel-Softmax function. Most importantly, Yu et al. (2020) first introduced the intuition of incorporating hardware constraints via an additive barrier penalty within such relaxed search frameworks, our work revisits these foundational assumptions by deriving the optimization objective directly from Lagrangian principles and perturbed Karush-Kuhn-Tucker conditions to develop a novel post-training algorithm.

3 Constrained Mixed Precision Search

Post-training compression While neural architecture search for mixed-precision models has mostly been developed as part of a quantization-aware training framework, Li et al. (2020) have shown that the optimal approach to model compression is to first train large networks in full precision, and then aggressively compress the model for deployment. By following this framework, we rework on the assumptions of the neural network bit-allocation problem. We propose to restrict the problem to the search of architectural parameters for pre-trained models, maintaining the previously learned weights W^* frozen. This significantly reduces the number of parameter updates, as the number of architecture parameters only grows linearly with the depth of the associated network and is invariant with respect to the dimensions of its layers. In turn, this allows us the use of a significantly smaller calibration dataset for the search phase.

User-defined architectural constraints In practical deployment scenarios, models must conform to diverse hardware constraints, including limits on total model size, supported numerical formats, and compute budgets such as FLOPs or BOPs. These constraints are platform-dependent and are often non-negotiable. To accommodate such deployment requirements, we reformulate the bit allocation task not as a multi-objective trade-off between accuracy and complexity, but as a constrained optimization problem. Let $\mathcal{C}(.)$ be a differentiable architectural cost function e.g., total model size in bits as follows:

$$\mathcal{C}(A) = \frac{\sum_{l=1}^{L} s_l \sum_{d=1}^{D} A_{l,d} b_d}{\sum_{l=1}^{L} s_l} \tag{5}$$

where L is the number of layers, D is the number of format choices, s_l is the number of parameters in layer l, b_d is the bit-width of format choice d, and $A_{l,d}$ is the continuous, relaxed weight for choosing format d for layer l.

And let B denote an upper bound imposed by the hardware (e.g., a target average bit-width). Our goal is to minimize the loss subject to this constraint:

$$\begin{aligned} \underset{A}{minimize} \quad & \mathcal{L}(A, \hat{W}^*) \\ subject\ to \quad & \mathcal{R}_B[A] = B - \mathcal{C}(A) \geq 0 \end{aligned} \tag{6}$$

This constrained formulation enables the principled integration of hardware-awareness into the precision allocation process, ensuring that the resulting architecture is both accurate and deployable.

Interior-Point Formulation To solve the non-linear constrained optimization problem defined in equation 6, we employ techniques common in constrained optimization, specifically adopting a barrier-based interior-point method. The first step involves formulating the Lagrangian function, which incorporates the objective function and the constraint scaled by a Lagrange multiplier λ:

$$\mathcal{L}_\lambda(A) = \mathcal{L}(A, \hat{W}^*) + \lambda \mathcal{R}_B[A] \tag{7}$$

Here, $\mathcal{L}(A, W^*)$ represents the original loss function (our objective to minimize) with fixed model weights W^*, and $\mathcal{R}_B[A]$ represents the hardware constraint function (which must be non-negative, $\mathcal{R}_B[A] \geq 0$). The variable λ is the Lagrange multiplier associated with this inequality constraint.

For a given candidate solution A^* to be a local optimum of the constrained problem equation 6 (under certain regularity conditions), it must satisfy the Karush-Kuhn-Tucker (KKT) conditions. These conditions are fundamental necessary conditions for optimality in nonlinear programming Boyd & Vandenberghen (2004). They generalize the method of Lagrange multipliers to handle inequality constraints. For our problem, the KKT conditions are:

$$\mathbf{KKT} \begin{cases} \nabla\mathcal{L}(A^*, \hat{W}^*) + \lambda\nabla_A\mathcal{R}_B[A^*] = 0 \quad \text{(Stationarity)} \\ \mathcal{R}_B[A^*] \geq 0 \quad \text{(Primal Feasibility)} \\ \lambda \geq 0 \quad \text{(Dual Feasibility)} \\ \lambda\mathcal{R}_B[A^*] = 0 \quad \text{(Complementary Slackness)} \end{cases} \tag{8}$$

However, in practice, satisfying the strict complementarity condition $\lambda\mathcal{R}_B[A^*] = 0$ leads to optimization challenges due to discontinuity at the boundary of the feasible region. To circumvent this, we adopt the perturbed KKT formulation, commonly used in interior point methods, which replaces the complementarity condition with a small nonzero slack μ.

$$\mathbf{KKT}(\mu) \begin{cases} \nabla\mathcal{L}(A^*, \hat{W}^*) + \lambda\nabla\mathcal{R}_B[A^*] = 0 \\ \mathcal{R}_B[A^*] \geq 0 \\ \lambda \geq 0 \\ \lambda\mathcal{R}_B[A^*] = -\mu \end{cases} \quad s.t. \quad \mu \to 0 \tag{9}$$

This relaxation smooths the boundary behavior of the optimizer and permits convergence to the constrained optimum from within the feasible set. Following this approximation, the Lagrange multiplier λ can be reformulated as:

$$\lambda = \frac{-\mu}{\mathcal{R}_B[A^*]} \tag{10}$$

Plugging λ into the gradient of equation 7 induces the gradient of a logarithmic function:

$$\nabla\mathcal{L}_\lambda(A, \hat{W}^*) = \nabla\mathcal{L}(A, \hat{W}^*) - \mu\nabla\mathcal{R}_B[A]\frac{1}{\mathcal{R}_B[A]} \tag{11}$$

It corresponds to minimizing the following barrier-augmented objective:

$$\underset{A}{\text{minimize}} \quad \mathcal{L}(A, W^*) - \mu\ln(\mathcal{R}_B[A]) \tag{12}$$

Here, the logarithmic barrier $\ln(\mathcal{R}_B[A])$ diverges to $-\infty$ as the constraint approaches 0, effectively discouraging the optimizer from leaving the feasible region. In the appendix, we also propose a surrogate constraint function $\hat{\mathcal{R}}$ to smooth out the search near the boundary of the feasible region.

Algorithm Following our previous derivation, we propose the following iterative algorithm.

To minimize the model loss while staying within region defined by the memory constraint, the interior-point method adds a logarithmic barrier penalty. This penalty acts like a repulsive force that becomes very large at the constraint boundary, ensuring the solution always remains strictly feasible prior to the rounding step, which may induce negligible variations. Optimization starts with a strong repulsion (large μ), keeping the solution near the center of the feasible region. As μ is gradually decreased across iterations, the barrier's influence weakens, allowing the solution to follow a "central path" closer to the true minimum of L while still being repelled from the boundary. The figure below illustrates how each step balances minimizing the objective (descent step) with staying feasible (step towards central path), ultimately converging to the constrained optimum as $\mu \to 0$.

Algorithm 1 Constrained Bit Allocation

Require: Pretrained weights W^*, initial (relaxed) allocation parameters $A^{(0)}$, calibration dataset $\mathcal{D}_{\text{cal}}$, loss function $\mathcal{L}(\cdot, \cdot; \mathcal{D}_{\text{cal}})$, softplus constraint surrogate $\mathcal{R}_B[\cdot]$, initial barrier weight $\mu > 0$, decay factor $0 < \delta < 1$, number of outer iterations T, number of inner epochs E, learning rate for A parameters η_A.

Ensure: Final discrete allocation $\hat{A}$ satisfying $C(\hat{A}) \leq B$

$t \leftarrow 1$
$\mu^{(1)} \leftarrow \mu$
$A \leftarrow A^{(0)}$
while $t \leq T$ **do**
  for $epoch = 1$ to E **do**
    $g_A \leftarrow \nabla_A \left[\mathcal{L}(A, \hat{W}^*; \mathcal{D}_{\text{cal}}) - \mu^{(t)} \ln\big(B - C(A)\big) \right]$
    $A \leftarrow A - \eta_A g_A$
  end for
  $\mu^{(t+1)} \leftarrow \delta \mu^{(t)}$
  $t \leftarrow t + 1$
end while
$\hat{A} \leftarrow \text{round}(A)$
return $\hat{A}$

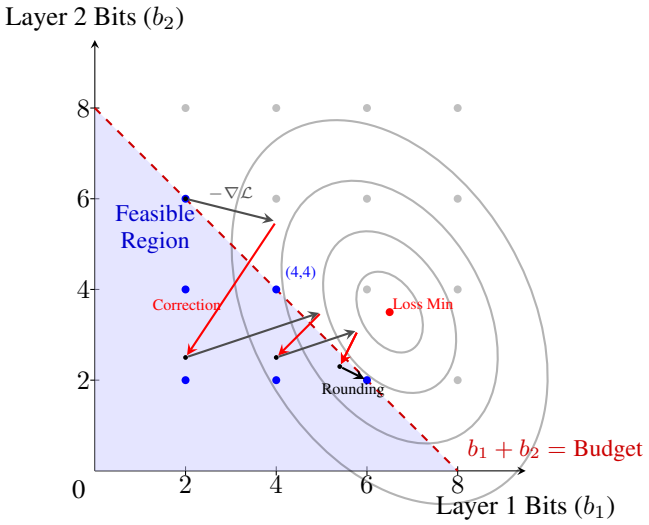

Figure 1: Search space for bit allocation in a 2-layer network. Axes are bits per layer (b_1, b_2). Blue dots are feasible discrete choices under a budget constraint (shaded region, $b_1 + b_2 \leq$ Budget). Gray dots are infeasible. Gray ellipses represent level curves of the loss function, with the true (continuous) minimum marked in red, located between discrete points.

4 Experimental Methodology and Results

To evaluate the effectiveness of our method, we conducted a series of post-training experiments on 10 transformer models of varying scales, including OPT (Zhang et al. (2022b)), LLaMA (Grattafiori et al. (2024)), Gemma (Team et al. (2024; 2025)), and Qwen (Team (2024a;b); Qwen et al. (2025)) architectures with up to 3 billion parameters. All experiments follow the setup for causal language modeling provided by the open-source examples of HuggingFace. Importantly, we operate strictly in the post-training regime: the model weights are frozen, and only the architectural parameters governing format assignment are optimized using a small calibration set. All models are adapted using a mixture of MX-compliant formats, specifically MXFP4 and MXFP8. All experiments were performed on a single GPU and mainly implemented using the PyTorch library, Huggingface's transformers library, and MXFP emulation library by Microsoft (2024).

Empirical study 1: few-shot scenario In the few-shot setting, we use a small calibration set of 128 samples drawn from the training split of the C4 corpus proposed by Dodge et al. (2021). We then evaluate perplexity (PPL) on the C4 validation split, gauging performance on in-distribution data under low-data conditions. Figure 2 compares the perplexity of our mixed-precision allocations constrained to an average of 4.5 bits ('Mixed', red cross) against uniform MXFP baselines. Remarkably, this technique, initially designed to amortize the performance degradation of low-precision quantization, demonstrates that a carefully constrained 4.5-bit allocation can be competitive with, and in some cases, even outperform higher-precision uniform allocations. For instance, Gemma-3-4B-it with our 4.5-bit mix surpasses both uniform MXFP6 and MXFP8 baselines on C4 perplexity. Significant perplexity improvements are also observed for Llama-3.2-1B (↓2.60) and Gemma-3B-it (↓3.67), with both models effectively closing the performance gap to their uniform MXFP6 counterparts despite our mixture being predominantly composed of MXFP4 tensors. Other notable improvements of over 5% perplexity reduction include OPT-350M (↓1.5 points) and Qwen2.5-0.5B (↓2.08 points) when compared to the MXFP4 baseline. These gains are achieved with only an approximate +0.25 effective bit increase.

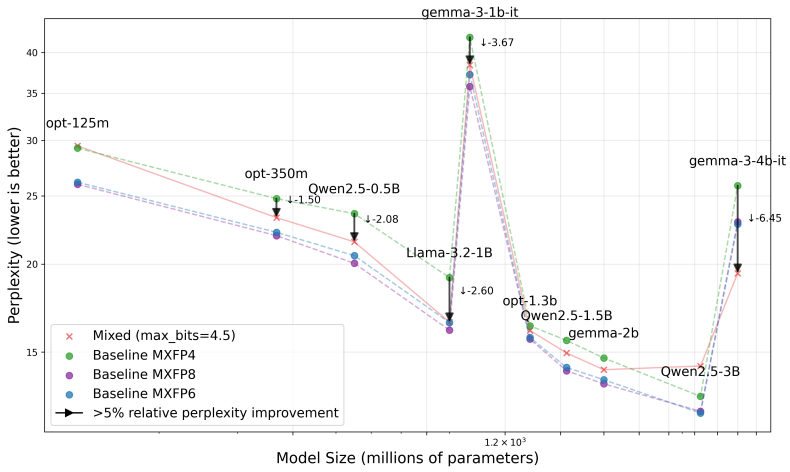

Figure 2: Few-shot perplexity (lower is better) on C4 validation set for models constrained to 4.5 bits. Our mixed allocation (red cross) is compared against uniform MXFP4, MXFP6, and MXFP8 baselines. Black arrows indicate perplexity improvements $\geq$ 5% improvements over the MXFP4 baseline.

Figure 3 shows the achieved effective bit-widths for the models under the 4.5-bit constraint. In 8 out of 10 models, the resulting effective bit-widths are strictly under the user-defined constraint. For OPT-125M and Qwen2.5-0.5B, the rounding step in the final allocation resulted in a slight increase, but the framework generally adheres closely to the target hardware budget, with most deviations being minor.

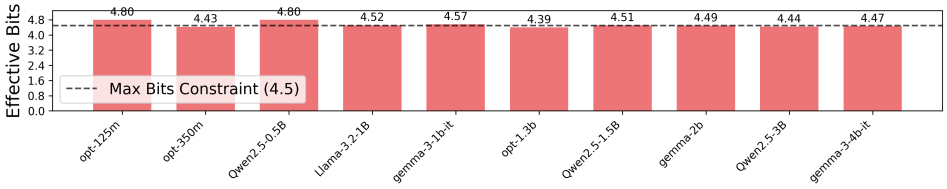

Figure 3: Effective bits achieved for models constrained to 4.5 bits in the few-shot setting. The dashed line indicates the target constraint.

Empirical study 2: zero-shot scenario For zero-shot evaluation, we calibrate using 256 samples from the C4 training split. We then employ the lm-eval-harness benchmark suite Biderman et al. (2024); Gao et al. (2024) to assess model performance on downstream tasks without task-specific

fine-tuning. We report accuracy on LAMBADA Paperno et al. (2016) (predicting the last word of a passage, testing context understanding) and perplexity on WikiText-2-raw (general language modeling capability) (Merity et al. (2016)).

Figure 4 presents LAMBADA accuracy for the 4.5-bit constraint. Our mixed allocation yields substantial accuracy improvements over the uniform MXFP4 baseline, including a striking +10.7% for Qwen2.5-0.5B. Other significant gains (exceeding two standard deviations) are seen for OPT-350M (+2.7%) and Gemma-3-1B-it (+3.8%), with the latter closing the gap to the MXFP6 baseline. Impressively, for Qwen2.5-1.5B, Gemma-2B, OPT-1.3B, and Qwen2.5-3B, our 4.5-bit mixed-precision models outperform both the uniform MXFP6 (6.25 bits) and MXFP8 (8.25 bits) baselines, showcasing the power of strategic bit allocation.

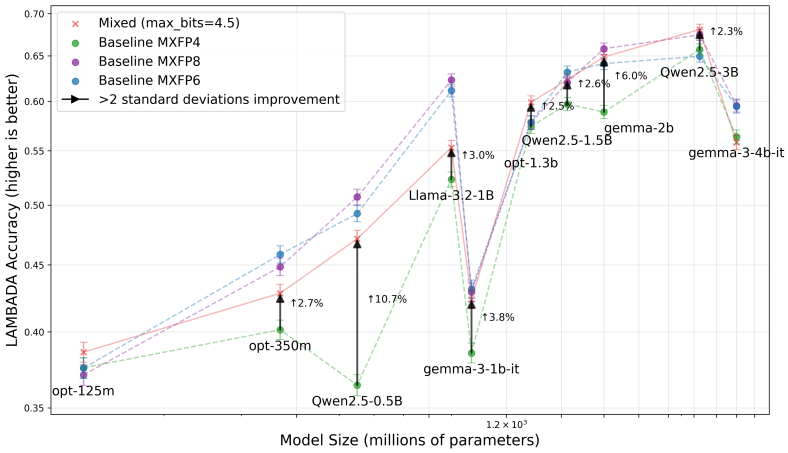

Figure 4: Zero-shot LAMBADA accuracy (higher is better) for models constrained to 4.5 bits. Our mixed allocation (red cross) compared against uniform baselines. Black arrows indicate accuracy improvement over MXFP4 baseline exceeding 2 standard deviations.

We further evaluate on WikiText perplexity (results shown in Figure 5). Consistent with other findings, we observe more than 5% perplexity improvements across the board. Notably, the Gemma family excels: Gemma-2B at 4.5 bits outperforms the MXFP4 baseline by 2.9 perplexity points and the MXFP6 baseline by over 45 points. Similar strong outperformance of the 6.25-bit MXFP6 baseline is seen with Gemma-3-1B-it (↓5.80 vs MXFP4) and Gemma-3-4B-it using only 4.5 effective bits. For other models, such as OPT-125M (↓3.31), OPT-350M (↓2.14), and Qwen2.5 (↓2.46), our method successfully closes the performance gap to higher-precision uniform allocations. These accuracy and perplexity improvements, achieved with frozen weights and calibration solely on C4 data, underscore the generalization capability of the learned allocations.

These zero-shot findings underscore that targeted precision allocation, guided by our constrained optimization, effectively preserves crucial model capabilities for downstream tasks. This approach often yields significantly better results than uniform low-bit formats, particularly under tighter memory constraints, and can even rival or exceed the performance of higher-precision uniform schemes. The method provides practitioners fine-grained control over the accuracy-compression trade-off simply by selecting the appropriate average bit-width constraint.

5 Discussions

Strengths A key strength of this methodology lies in its combined practicality, efficiency, and theoretical robustness. The entire allocation process operates post-training, requiring no modification or fine-tuning of the original model weights, which significantly reduces computational cost and technical complexity. Furthermore, its reliance on a remarkably small number of calibration samples (e.g., 128-256) and minimal runtime (down to 2.5 minutes for OPT-125M and up to 32 minutes for Gemma-3-4B) makes it highly feasible even with limited data access. Despite this efficiency, the derived allocations exhibit robust generalization, improving performance on both in-distribution

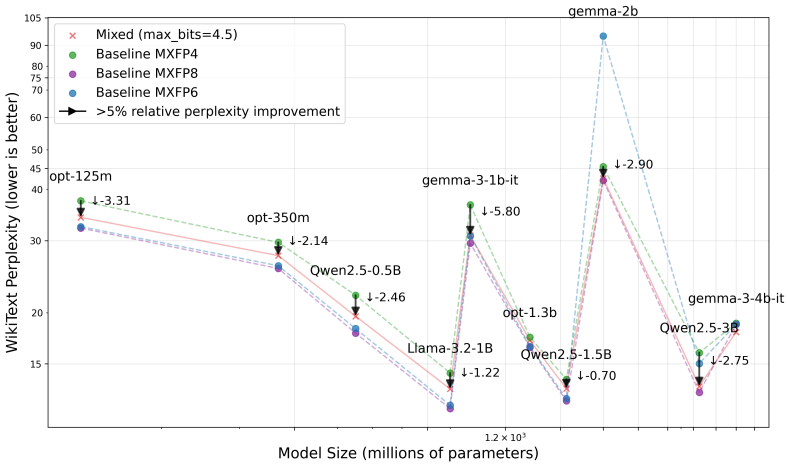

Figure 5: Zero-shot wikitext perplexity (lower is better) for models constrained to 4.5 bits. Our mixed allocation (red cross) compared against uniform baselines.

and diverse zero-shot tasks. From a theoretical standpoint, formulating the problem as a constrained optimization provides a more rigorous foundation than heuristic or multi-objective techniques lacking strong guarantees or requiring complex Pareto front analysis. The well-established interior-point method, applied with an average bit-width constraint, offers an interpretable way to directly incorporate hardware budgets.

Limitations We acknowledge certain limitations. The current approach implicitly utilizes a "supernet" concept during the search phase, where gradients for different format assignments are needed. This can temporarily increase memory usage during the allocation optimization compared to standard inference. However, the search often involves low-bit formats; the memory required to hold activations or gradients for multiple low-bit options might still be comparable to, or less than, holding a single higher-precision (e.g., FP16 or BF16) baseline tensor.

Future work Optimizing the memory of the supernet and the computational efficiency of the allocation search itself presents a viable avenue for future research. Investigating the interplay between different types of constraints (e.g., latency-aware constraints) and granularity (e.g., column-wise rather than layer-wise) within this framework is another promising direction.

Societal Impact By enabling more efficient deployment of large neural networks, this work contributes to reducing the energy consumption and computational resources required for AI model inference. This can lead to more sustainable AI practices and broader accessibility to advanced AI capabilities on less powerful hardware, potentially mitigating environmental impact and democratizing access to technology.

6 Conclusion

The escalating complexity of deep neural networks demands efficient deployment on resource-constrained hardware. While mixed-precision formats offer substantial potential, optimal layer-wise allocation under hardware constraints has remained a key challenge, often addressed by heuristics or training-aware searches. This paper introduced a principled, post-training framework for mixed-precision allocation grounded in constrained optimization theory. Our interior-point method directly incorporates hardware limitations, like memory footprint via average bit-width constraints, using only small calibration datasets and without requiring model retraining. Empirical evaluations across diverse transformer architectures demonstrate that strategic allocation, even with a limited set of precision formats (e.g., MXFP4 and MXFP8), bridges performance gaps between intermediate-precision formats (e.g., MXFP6), and can even outperform high-precision configurations.

REFERENCES

Stella Biderman, Hailey Schoelkopf, Lintang Sutawika, Leo Gao, Jonathan Tow, Baber Abbasi, Alham Fikri Aji, Pawan Sasanka Ammanamanchi, Sidney Black, Jordan Clive, Anthony DiPofi, Julen Etxaniz, Benjamin Fattori, Jessica Zosa Forde, Charles Foster, Jeffrey Hsu, Mimansa Jaiswal, Wilson Y. Lee, Haonan Li, Charles Lovering, Niklas Muennighoff, Ellie Pavlick, Jason Phang, Aviya Skowron, Samson Tan, Xiangru Tang, Kevin A. Wang, Genta Indra Winata, François Yvon, and Andy Zou. Lessons from the trenches on reproducible evaluation of language models, 2024. URL https://arxiv.org/abs/2405.14782.

Stephen Boyd and Lieven Vandenberghen. *Convex Optimization*. Cambridge University Press, 2004.

Zhaowei Cai and Nuno Vasconcelos. Rethinking differentiable search for mixed-precision neural networks. In *Proceedings of the IEEE/CVF Conference on Computer Vision and Pattern Recognition (CVPR)*, June 2020.

Zhaowei Cai and Nuno Vasconcelos. Edmips: Differentiable search of mixed precision networks for edge devices. In *2021 IEEE International Conference on Image Processing (ICIP)*, pp. 319–323. IEEE, 2021.

Peter Clark, Isaac Cowhey, Oren Etzioni, Tushar Khot, Ashish Sabharwal, Carissa Schoenick, and Oyvind Tafjord. Think you have solved question answering? try arc, the ai2 reasoning challenge. *arXiv preprint arXiv:1803.05457*, 2018.

Bita Darvish Rouhani, Ritchie Zhao, Venmugil Elango, Rasoul Shafipour, Mathew Hall, Maral Mesmakhosroshahi, Ankit More, Levi Melnick, Maximilian Golub, Girish Varatkar, et al. With shared microexponents, a little shifting goes a long way. In *Proceedings of the 50th Annual International Symposium on Computer Architecture*, pp. 1–13, 2023.

Tim Dettmers, Mike Lewis, Younes Belkada, and Luke Zettlemoyer. Llm.int8(): 8-bit matrix multiplication for transformers at scale, 2022. URL https://arxiv.org/abs/2208.07339.

Jesse Dodge, Maarten Sap, Ana Marasović, William Agnew, Gabriel Ilharco, Dirk Groeneveld, Margaret Mitchell, and Matt Gardner. Documenting large webtext corpora: A case study on the colossal clean crawled corpus, 2021. URL https://arxiv.org/abs/2104.08758.

Mario Drumond, Tao Lin, Martin Jaggi, and Babak Falsafi. Training dnns with hybrid block floating point. *Advances in Neural Information Processing Systems*, 31, 2018.

Leo Gao, Jonathan Tow, Baber Abbasi, Stella Biderman, Sid Black, Anthony DiPofi, Charles Foster, Laurence Golding, Jeffrey Hsu, Alain LeNac'h, Haonan Li, Kyle McDonell, Niklas Muennighoff, Chris Ociepa, Jason Phang, Laria Reynolds, Hailey Schoelkopf, Aviya Skowron, Lintang Sutawika, Eric Tang, Anish Thite, Ben Wang, Kevin Wang, and Andy Zou. A framework for few-shot language model evaluation, 2024.

Amir Gholami, Sehoon Kim, Zhen Dong, Zhewei Yao, Michael W. Mahoney, and Kurt Keutzer. A survey of quantization methods for efficient neural network inference, 2021. URL https://arxiv.org/abs/2103.13630.

Aaron Grattafiori, Abhimanyu Dubey, Abhinav Jauhri, Abhinav Pandey, Abhishek Kadian, Ahmad Al-Dahle, Aiesha Letman, Akhil Mathur, Alan Schelten, Alex Vaughan, Amy Yang, Angela Fan, Anirudh Goyal, Anthony Hartshorn, Aobo Yang, Archi Mitra, Archie Sravankumar, Artem Korenev, Arthur Hinsvark, Arun Rao, Aston Zhang, Aurelien Rodriguez, Austen Gregerson, Ava Spataru, Baptiste Roziere, Bethany Biron, Binh Tang, Bobbie Chern, Charlotte Caucheteux, Chaya Nayak, Chloe Bi, Chris Marra, Chris McConnell, Christian Keller, Christophe Touret, Chunyang Wu, Corinne Wong, Cristian Canton Ferrer, Cyrus Nikolaidis, Damien Allonsius, Daniel Song, Danielle Pintz, Danny Livshits, Danny Wyatt, David Esiobu, Dhruv Choudhary, Dhruv Mahajan, Diego Garcia-Olano, Diego Perino, Dieuwke Hupkes, Egor Lakomkin, Ehab AlBadawy, Elina Lobanova, Emily Dinan, Eric Michael Smith, Filip Radenovic, Francisco Guzmán, Frank Zhang, Gabriel Synnaeve, Gabrielle Lee, Georgia Lewis Anderson, Govind Thattai, Graeme Nail, Gregoire Mialon, Guan Pang, Guillem Cucurell, Hailey Nguyen, Hannah Korevaar, Hu Xu, Hugo Touvron, Iliyan Zarov, Imanol Arrieta Ibarra, Isabel Kloumann, Ishan Misra,

Ivan Evtimov, Jack Zhang, Jade Copet, Jaewon Lee, Jan Geffert, Jana Vranes, Jason Park, Jay Mahadeokar, Jeet Shah, Jelmer van der Linde, Jennifer Billock, Jenny Hong, Jenya Lee, Jeremy Fu, Jianfeng Chi, Jianyu Huang, Jiawen Liu, Jie Wang, Jiecao Yu, Joanna Bitton, Joe Spisak, Jongsoo Park, Joseph Rocca, Joshua Johnstun, Joshua Saxe, Junteng Jia, Kalyan Vasuden Alwala, Karthik Prasad, Kartikeya Upasani, Kate Plawiak, Ke Li, Kenneth Heafield, Kevin Stone, Khalid El-Arini, Krithika Iyer, Kshitiz Malik, Kuenley Chiu, Kunal Bhalla, Kushal Lakhotia, Lauren Rantala-Yeary, Laurens van der Maaten, Lawrence Chen, Liang Tan, Liz Jenkins, Louis Martin, Lovish Madaan, Lubo Malo, Lukas Blecher, Lukas Landzaat, Luke de Oliveira, Madeline Muzzi, Mahesh Pasupuleti, Mannat Singh, Manohar Paluri, Marcin Kardas, Maria Tsimpoukelli, Mathew Oldham, Mathieu Rita, Maya Pavlova, Melanie Kambadur, Mike Lewis, Min Si, Mitesh Kumar Singh, Mona Hassan, Naman Goyal, Narjes Torabi, Nikolay Bashlykov, Nikolay Bogoychev, Niladri Chatterji, Ning Zhang, Olivier Duchenne, Onur Çelebi, Patrick Alrassy, Pengchuan Zhang, Pengwei Li, Petar Vasic, Peter Weng, Prajjwal Bhargava, Pratik Dubal, Praveen Krishnan, Punit Singh Koura, Puxin Xu, Qing He, Qingxiao Dong, Ragavan Srinivasan, Raj Ganapathy, Ramon Calderer, Ricardo Silveira Cabral, Robert Stojnic, Roberta Raileanu, Rohan Maheswari, Rohit Girdhar, Rohit Patel, Romain Sauvestre, Ronnie Polidoro, Roshan Sumbaly, Ross Taylor, Ruan Silva, Rui Hou, Rui Wang, Saghar Hosseini, Sahana Chennabasappa, Sanjay Singh, Sean Bell, Seohyun Sonia Kim, Sergey Edunov, Shaoliang Nie, Sharan Narang, Sharath Raparthy, Sheng Shen, Shengye Wan, Shruti Bhosale, Shun Zhang, Simon Vandenhende, Soumya Batra, Spencer Whitman, Sten Sootla, Stephane Collot, Suchin Gururangan, Sydney Borodinsky, Tamar Herman, Tara Fowler, Tarek Sheasha, Thomas Georgiou, Thomas Scialom, Tobias Speckbacher, Todor Mihaylov, Tong Xiao, Ujjwal Karn, Vedanuj Goswami, Vibhor Gupta, Vignesh Ramanathan, Viktor Kerkez, Vincent Gonguet, Virginie Do, Vish Vogeti, Vítor Albiero, Vladan Petrovic, Weiwei Chu, Wenhan Xiong, Wenyin Fu, Whitney Meers, Xavier Martinet, Xiaodong Wang, Xiaofang Wang, Xiaoqing Ellen Tan, Xide Xia, Xinfeng Xie, Xuchao Jia, Xuewei Wang, Yaelle Goldschlag, Yashesh Gaur, Yasmine Babaei, Yi Wen, Yiwen Song, Yuchen Zhang, Yue Li, Yuning Mao, Zacharie Delpierre Coudert, Zheng Yan, Zhengxing Chen, Zoe Papakipos, Aaditya Singh, Aayushi Srivastava, Abha Jain, Adam Kelsey, Adam Shajnfeld, Adithya Gangidi, Adolfo Victoria, Ahuva Goldstand, Ajay Menon, Ajay Sharma, Alex Boesenberg, Alexei Baevski, Allie Feinstein, Amanda Kallet, Amit Sangani, Amos Teo, Anam Yunus, Andrei Lupu, Andres Alvarado, Andrew Caples, Andrew Gu, Andrew Ho, Andrew Poulton, Andrew Ryan, Ankit Ramchandani, Annie Dong, Annie Franco, Anuj Goyal, Aparajita Saraf, Arkabandhu Chowdhury, Ashley Gabriel, Ashwin Bharambe, Assaf Eisenman, Azadeh Yazdan, Beau James, Ben Maurer, Benjamin Leonhardi, Bernie Huang, Beth Loyd, Beto De Paola, Bhargavi Paranjape, Bing Liu, Bo Wu, Boyu Ni, Braden Hancock, Bram Wasti, Brandon Spence, Brani Stojkovic, Brian Gamido, Britt Montalvo, Carl Parker, Carly Burton, Catalina Mejia, Ce Liu, Changhan Wang, Changkyu Kim, Chao Zhou, Chester Hu, Ching-Hsiang Chu, Chris Cai, Chris Tindal, Christoph Feichtenhofer, Cynthia Gao, Damon Civin, Dana Beaty, Daniel Kreymer, Daniel Li, David Adkins, David Xu, Davide Testuggine, Delia David, Devi Parikh, Diana Liskovich, Didem Foss, Dingkang Wang, Duc Le, Dustin Holland, Edward Dowling, Eissa Jamil, Elaine Montgomery, Eleonora Presani, Emily Hahn, Emily Wood, Eric-Tuan Le, Erik Brinkman, Esteban Arcaute, Evan Dunbar, Evan Smothers, Fei Sun, Felix Kreuk, Feng Tian, Filippos Kokkinos, Firat Ozgenel, Francesco Caggioni, Frank Kanayet, Frank Seide, Gabriela Medina Florez, Gabriella Schwarz, Gada Badeer, Georgia Swee, Gil Halpern, Grant Herman, Grigory Sizov, Guangyi, Zhang, Guna Lakshminarayanan, Hakan Inan, Hamid Shojanazeri, Han Zou, Hannah Wang, Hanwen Zha, Haroun Habeeb, Harrison Rudolph, Helen Suk, Henry Aspegren, Hunter Goldman, Hongyuan Zhan, Ibrahim Damlaj, Igor Molybog, Igor Tufanov, Ilias Leontiadis, Irina-Elena Veliche, Itai Gat, Jake Weissman, James Geboski, James Kohli, Janice Lam, Japhet Asher, Jean-Baptiste Gaya, Jeff Marcus, Jeff Tang, Jennifer Chan, Jenny Zhen, Jeremy Reizenstein, Jeremy Teboul, Jessica Zhong, Jian Jin, Jingyi Yang, Joe Cummings, Jon Carvill, Jon Shepard, Jonathan McPhie, Jonathan Torres, Josh Ginsburg, Junjie Wang, Kai Wu, Kam Hou U, Karan Saxena, Kartikay Khandelwal, Katayoun Zand, Kathy Matosich, Kaushik Veeraraghavan, Kelly Michelena, Keqian Li, Kiran Jagadeesh, Kun Huang, Kunal Chawla, Kyle Huang, Lailin Chen, Lakshya Garg, Lavender A, Leandro Silva, Lee Bell, Lei Zhang, Liangpeng Guo, Licheng Yu, Liron Moshkovich, Luca Wehrstedt, Madian Khabsa, Manav Avalani, Manish Bhatt, Martynas Mankus, Matan Hasson, Matthew Lennie, Matthias Reso, Maxim Groshev, Maxim Naumov, Maya Lathi, Meghan Keneally, Miao Liu, Michael L. Seltzer, Michal Valko, Michelle Restrepo, Mihir Patel, Mik Vyatskov, Mikayel Samvelyan, Mike Clark, Mike Macey, Mike Wang, Miquel Jubert Hermoso, Mo Metanat, Mohammad Rastegari, Munish Bansal, Nandhini Santhanam, Natascha Parks, Natasha White, Navyata Bawa, Nayan

Singhal, Nick Egebo, Nicolas Usunier, Nikhil Mehta, Nikolay Pavlovich Laptev, Ning Dong, Norman Cheng, Oleg Chernoguz, Olivia Hart, Omkar Salpekar, Ozlem Kalinli, Parkin Kent, Parth Parekh, Paul Saab, Pavan Balaji, Pedro Rittner, Philip Bontrager, Pierre Roux, Piotr Dollar, Polina Zvyagina, Prashant Ratanchandani, Pritish Yuvraj, Qian Liang, Rachad Alao, Rachel Rodriguez, Rafi Ayub, Raghotham Murthy, Raghu Nayani, Rahul Mitra, Rangaprabhu Parthasarathy, Raymond Li, Rebekkah Hogan, Robin Battey, Rocky Wang, Russ Howes, Ruty Rinott, Sachin Mehta, Sachin Siby, Sai Jayesh Bondu, Samyak Datta, Sara Chugh, Sara Hunt, Sargun Dhillon, Sasha Sidorov, Satadru Pan, Saurabh Mahajan, Saurabh Verma, Seiji Yamamoto, Sharadh Ramaswamy, Shaun Lindsay, Shaun Lindsay, Sheng Feng, Shenghao Lin, Shengxin Cindy Zha, Shishir Patil, Shiva Shankar, Shuqiang Zhang, Shuqiang Zhang, Sinong Wang, Sneha Agarwal, Soji Sajuyigbe, Soumith Chintala, Stephanie Max, Stephen Chen, Steve Kehoe, Steve Satterfield, Sudarshan Govindaprasad, Sumit Gupta, Summer Deng, Sungmin Cho, Sunny Virk, Suraj Subramanian, Sy Choudhury, Sydney Goldman, Tal Remez, Tamar Glaser, Tamara Best, Thilo Koehler, Thomas Robinson, Tianhe Li, Tianjun Zhang, Tim Matthews, Timothy Chou, Tzook Shaked, Varun Vontimitta, Victoria Ajayi, Victoria Montanez, Vijai Mohan, Vinay Satish Kumar, Vishal Mangla, Vlad Ionescu, Vlad Poenaru, Vlad Tiberiu Mihailescu, Vladimir Ivanov, Wei Li, Wenchen Wang, Wenwen Jiang, Wes Bouaziz, Will Constable, Xiaocheng Tang, Xiaojian Wu, Xiaolan Wang, Xilun Wu, Xinbo Gao, Yaniv Kleinman, Yanjun Chen, Ye Hu, Ye Jia, Ye Qi, Yenda Li, Yilin Zhang, Ying Zhang, Yossi Adi, Youngjin Nam, Yu, Wang, Yu Zhao, Yuchen Hao, Yundi Qian, Yunlu Li, Yuzi He, Zach Rait, Zachary DeVito, Zef Rosnbrick, Zhaoduo Wen, Zhenyu Yang, Zhiwei Zhao, and Zhiyu Ma. The llama 3 herd of models, 2024. URL https://arxiv.org/abs/2407.21783.

Benoit Jacob, Skirmantas Kligys, Bo Chen, Menglong Zhu, Matthew Tang, Andrew Howard, Hartwig Adam, and Dmitry Kalenichenko. Quantization and training of neural networks for efficient integer-arithmetic-only inference. In *Proceedings of the IEEE Conference on Computer Vision and Pattern Recognition (CVPR)*, June 2018.

Changhun Lee, Jungyu Jin, Taesu Kim, Hyungjun Kim, and Eunhyeok Park. Owq: Outlier-aware weight quantization for efficient fine-tuning and inference of large language models. In *Proceedings of the AAAI Conference on Artificial Intelligence*, volume 38, pp. 13355–13364, 2024.

Zhuohan Li, Eric Wallace, Sheng Shen, Kevin Lin, Kurt Keutzer, Dan Klein, and Joseph E. Gonzalez. Train large, then compress: Rethinking model size for efficient training and inference of transformers, 2020. URL https://arxiv.org/abs/2002.11794.

Stephen Merity, Caiming Xiong, James Bradbury, and Richard Socher. Pointer sentinel mixture models, 2016. URL https://arxiv.org/abs/1609.07843.

Paulius Micikevicius, Dusan Stosic, Neil Burgess, Marius Cornea, Pradeep Dubey, Richard Grisenthwaite, Sangwon Ha, Alexander Heinecke, Patrick Judd, John Kamalu, et al. Fp8 formats for deep learning. In *arXiv preprint arXiv:2209.05433*, 2022.

Microsoft. Mx pytorch emulation library. https://github.com/microsoft/microxcaling, 2024.

MLCommons. Mlperf inference benchmark. https://mlcommons.org/en/inference-overview/, a. Accessed: 2025-09-11.

MLCommons. Mlperf training benchmark. https://mlcommons.org/en/training-overview/, b. Accessed: 2025-09-11.

Jorge Nocedal and Stephen Wright. *Numerical Optimization*. Springer Series in Operations Research and Financial Engineering. Springer Science & Business Media, 2006.

Open Compute Project. Ocp microscaling formats (mx) specification version 1.0. Technical report, Open Compute Project, 2023. URL https://www.opencompute.org. Defines MXFP8/6/4 and MXINT8 formats for AI hardware.

Denis Paperno, Germán Kruszewski, Angeliki Lazaridou, Quan Ngoc Pham, Raffaella Bernardi, Sandro Pezzelle, Marco Baroni, Gemma Boleda, and Raquel Fernández. The lambada dataset: Word prediction requiring a broad discourse context. In *Proceedings of the 54th Annual Meeting of the Association for Computational Linguistics (Volume 1: Long Papers)*, 2016.

Qwen, :, An Yang, Baosong Yang, Beichen Zhang, Binyuan Hui, Bo Zheng, Bowen Yu, Chengyuan Li, Dayiheng Liu, Fei Huang, Haoran Wei, Huan Lin, Jian Yang, Jianhong Tu, Jianwei Zhang, Jianxin Yang, Jiaxi Yang, Jingren Zhou, Junyang Lin, Kai Dang, Keming Lu, Keqin Bao, Kexin Yang, Le Yu, Mei Li, Mingfeng Xue, Pei Zhang, Qin Zhu, Rui Men, Runji Lin, Tianhao Li, Tianyi Tang, Tingyu Xia, Xingzhang Ren, Xuancheng Ren, Yang Fan, Yang Su, Yichang Zhang, Yu Wan, Yuqiong Liu, Zeyu Cui, Zhenru Zhang, and Zihan Qiu. Qwen2.5 technical report, 2025. URL https://arxiv.org/abs/2412.15115.

Bita Darvish Rouhani, Ritchie Zhao, Ankit More, Mathew Hall, Alireza Khodamoradi, Summer Deng, Dhruv Choudhary, Marius Cornea, Eric Dellinger, Kristof Denolf, Stosic Dusan, Venmugil Elango, Maximilian Golub, Alexander Heinecke, Phil James-Roxby, Dharmesh Jani, Gaurav Kolhe, Martin Langhammer, Ada Li, Levi Melnick, Maral Mesmakhosroshahi, Andres Rodriguez, Michael Schulte, Rasoul Shafipour, Lei Shao, Michael Siu, Pradeep Dubey, Paulius Micikevicius, Maxim Naumov, Colin Verrilli, Ralph Wittig, Doug Burger, and Eric Chung. Microscaling data formats for deep learning, 2023. URL https://arxiv.org/abs/2310.10537.

Ebby Samson, Naveen Mellempudi, Wayne Luk, and George A. Constantinides. Exploring fpga designs for mx and beyond, 2024. URL https://arxiv.org/abs/2407.01475.

Gemma Team, Thomas Mesnard, Cassidy Hardin, Robert Dadashi, Surya Bhupatiraju, Shreya Pathak, Laurent Sifre, Morgane Rivière, Mihir Sanjay Kale, Juliette Love, Pouya Tafti, Léonard Hussenot, Pier Giuseppe Sessa, Aakanksha Chowdhery, Adam Roberts, Aditya Barua, Alex Botev, Alex Castro-Ros, Ambrose Slone, Amélie Héliou, Andrea Tacchetti, Anna Bulanova, Antonia Paterson, Beth Tsai, Bobak Shahriari, Charline Le Lan, Christopher A. Choquette-Choo, Clément Crepy, Daniel Cer, Daphne Ippolito, David Reid, Elena Buchatskaya, Eric Ni, Eric Noland, Geng Yan, George Tucker, George-Christian Muraru, Grigory Rozhdestvenskiy, Henryk Michalewski, Ian Tenney, Ivan Grishchenko, Jacob Austin, James Keeling, Jane Labanowski, Jean-Baptiste Lespiau, Jeff Stanway, Jenny Brennan, Jeremy Chen, Johan Ferret, Justin Chiu, Justin Mao-Jones, Katherine Lee, Kathy Yu, Katie Millican, Lars Lowe Sjoesund, Lisa Lee, Lucas Dixon, Machel Reid, Maciej Mikuła, Mateo Wirth, Michael Sharman, Nikolai Chinaev, Nithum Thain, Olivier Bachem, Oscar Chang, Oscar Wahltinez, Paige Bailey, Paul Michel, Petko Yotov, Rahma Chaabouni, Ramona Comanescu, Reena Jana, Rohan Anil, Ross McIlroy, Ruibo Liu, Ryan Mullins, Samuel L Smith, Sebastian Borgeaud, Sertan Girgin, Sholto Douglas, Shree Pandya, Siamak Shakeri, Soham De, Ted Klimenko, Tom Hennigan, Vlad Feinberg, Wojciech Stokowiec, Yu hui Chen, Zafarali Ahmed, Zhitao Gong, Tris Warkentin, Ludovic Peran, Minh Giang, Clément Farabet, Oriol Vinyals, Jeff Dean, Koray Kavukcuoglu, Demis Hassabis, Zoubin Ghahramani, Douglas Eck, Joelle Barral, Fernando Pereira, Eli Collins, Armand Joulin, Noah Fiedel, Evan Senter, Alek Andreev, and Kathleen Kenealy. Gemma: Open models based on gemini research and technology, 2024. URL https://arxiv.org/abs/2403.08295.

Gemma Team, Aishwarya Kamath, Johan Ferret, Shreya Pathak, Nino Vieillard, Ramona Merhej, Sarah Perrin, Tatiana Matejovicova, Alexandre Ramé, Morgane Rivière, Louis Rouillard, Thomas Mesnard, Geoffrey Cideron, Jean bastien Grill, Sabela Ramos, Edouard Yvinec, Michelle Casbon, Etienne Pot, Ivo Penchev, Gaël Liu, Francesco Visin, Kathleen Kenealy, Lucas Beyer, Xiaohai Zhai, Anton Tsitsulin, Robert Busa-Fekete, Alex Feng, Noveen Sachdeva, Benjamin Coleman, Yi Gao, Basil Mustafa, Iain Barr, Emilio Parisotto, David Tian, Matan Eyal, Colin Cherry, Jan-Thorsten Peter, Danila Sinopalnikov, Surya Bhupatiraju, Rishabh Agarwal, Mehran Kazemi, Dan Malkin, Ravin Kumar, David Vilar, Idan Brusilovsky, Jiaming Luo, Andreas Steiner, Abe Friesen, Abhanshu Sharma, Abheesht Sharma, Adi Mayrav Gilady, Adrian Goedeckemeyer, Alaa Saade, Alex Feng, Alexander Kolesnikov, Alexei Bendebury, Alvin Abdagic, Amit Vadi, András György, André Susano Pinto, Anil Das, Ankur Bapna, Antoine Miech, Antoine Yang, Antonia Paterson, Ashish Shenoy, Ayan Chakrabarti, Bilal Piot, Bo Wu, Bobak Shahriari, Bryce Petrini, Charlie Chen, Charline Le Lan, Christopher A. Choquette-Choo, CJ Carey, Cormac Brick, Daniel Deutsch, Danielle Eisenbud, Dee Cattle, Derek Cheng, Dimitris Paparas, Divyashree Shivakumar Sreepathihalli, Doug Reid, Dustin Tran, Dustin Zelle, Eric Noland, Erwin Huizenga, Eugene Kharitonov, Frederick Liu, Gagik Amirkhanyan, Glenn Cameron, Hadi Hashemi, Hanna Klimczak-Plucińska, Harman Singh, Harsh Mehta, Harshal Tushar Lehri, Hussein Hazimeh, Ian Ballantyne, Idan Szpektor, Ivan Nardini, Jean Pouget-Abadie, Jetha Chan, Joe Stanton, John Wieting, Jonathan Lai, Jordi Orbay, Joseph Fernandez, Josh Newlan, Ju yeong Ji, Jyotinder Singh,

Kat Black, Kathy Yu, Kevin Hui, Kiran Vodrahalli, Klaus Greff, Linhai Qiu, Marcella Valentine, Marina Coelho, Marvin Ritter, Matt Hoffman, Matthew Watson, Mayank Chaturvedi, Michael Moynihan, Min Ma, Nabila Babar, Natasha Noy, Nathan Byrd, Nick Roy, Nikola Momchev, Nilay Chauhan, Noveen Sachdeva, Oskar Bunyan, Pankil Botarda, Paul Caron, Paul Kishan Rubenstein, Phil Culliton, Philipp Schmid, Pier Giuseppe Sessa, Pingmei Xu, Piotr Stanczyk, Pouya Tafti, Rakesh Shivanna, Renjie Wu, Renke Pan, Reza Rokni, Rob Willoughby, Rohith Vallu, Ryan Mullins, Sammy Jerome, Sara Smoot, Sertan Girgin, Shariq Iqbal, Shashir Reddy, Shruti Sheth, Siim Põder, Sijal Bhatnagar, Sindhu Raghuram Panyam, Sivan Eiger, Susan Zhang, Tianqi Liu, Trevor Yacovone, Tyler Liechty, Uday Kalra, Utku Evci, Vedant Misra, Vincent Roseberry, Vlad Feinberg, Vlad Kolesnikov, Woohyun Han, Woosuk Kwon, Xi Chen, Yinlam Chow, Yuvein Zhu, Zichuan Wei, Zoltan Egyed, Victor Cotruta, Minh Giang, Phoebe Kirk, Anand Rao, Kat Black, Nabila Babar, Jessica Lo, Erica Moreira, Luiz Gustavo Martins, Omar Sanseviero, Lucas Gonzalez, Zach Gleicher, Tris Warkentin, Vahab Mirrokni, Evan Senter, Eli Collins, Joelle Barral, Zoubin Ghahramani, Raia Hadsell, Yossi Matias, D. Sculley, Slav Petrov, Noah Fiedel, Noam Shazeer, Oriol Vinyals, Jeff Dean, Demis Hassabis, Koray Kavukcuoglu, Clement Farabet, Elena Buchatskaya, Jean-Baptiste Alayrac, Rohan Anil, Dmitry, Lepikhin, Sebastian Borgeaud, Olivier Bachem, Armand Joulin, Alek Andreev, Cassidy Hardin, Robert Dadashi, and Léonard Hussenot. Gemma 3 technical report, 2025. URL https://arxiv.org/abs/2503.19786.

Qwen Team. Qwen1.5: Advancing Large Language Models via improved training, scaling, and post-training methodologies, 2024a.

Qwen Team. Qwen2: A family of strong and versatile language models, 2024b.

Alvin Wan, Xiaoliang Dai, Peizhao Zhang, Zijian He, Yuandong Tian, Saining Xie, Bichen Wu, Matthew Yu, Tao Xu, Kan Chen, et al. Fbnetv2: Differentiable neural architecture search for spatial and channel dimensions. In *Proceedings of the IEEE/CVF conference on computer vision and pattern recognition*, pp. 12965–12974, 2020.

Bichen Wu, Yanghan Wang, Peizhao Zhang, Yuandong Tian, Peter Vajda, and Kurt Keutzer. Mixed precision quantization of convnets via differentiable neural architecture search, 2018. URL https://arxiv.org/abs/1812.00090.

Bichen Wu, Xiaoliang Dai, Peizhao Zhang, Yanghan Wang, Fei Sun, Yiming Wu, Yuandong Tian, Peter Vajda, Yangqing Jia, and Kurt Keutzer. Fbnet: Hardware-aware efficient convnet design via differentiable neural architecture search. In *Proceedings of the IEEE/CVF conference on computer vision and pattern recognition*, pp. 10734–10742, 2019.

Haibao Yu, Qi Han, Jianbo Li, Jianping Shi, Guangliang Cheng, and Bin Fan. Search what you want: Barrier panelty nas for mixed precision quantization. In Andrea Vedaldi, Horst Bischof, Thomas Brox, and Jan-Michael Frahm (eds.), *Computer Vision – ECCV 2020*, pp. 1–16, Cham, 2020. Springer International Publishing. ISBN 978-3-030-58545-7.

Chiyuan Zhang, Samy Bengio, and Yoram Singer. Are all layers created equal?, 2022a. URL https://arxiv.org/abs/1902.01996.

Susan Zhang, Stephen Roller, Naman Goyal, Mikel Artetxe, Moya Chen, Shuohui Chen, Christopher Dewan, Mona Diab, Xian Li, Xi Victoria Lin, Todor Mihaylov, Myle Ott, Sam Shleifer, Kurt Shuster, Daniel Simig, Punit Singh Koura, Anjali Sridhar, Tianlu Wang, and Luke Zettlemoyer. Opt: Open pre-trained transformer language models, 2022b. URL https://arxiv.org/abs/2205.01068.

A HEURISTIC SURROGATE FUNCTION FOR SMOOTHER SEARCH

The optimization of architectural parameters A using stochastic gradient descent based optimizers for our constrained bit allocation problem introduces a practical challenge. The logarithmic barrier term, $-\mu \ln(\mathcal{R}_B[A])$, where $\mathcal{R}_B[A] = B - C(A, W^*)$ is the constraint function, is undefined or tends to $-\infty$ if the constraint is violated (i.e., if $C(A, W^*) \geq B$, making $\mathcal{R}_B[A] \leq 0$). With SGD, due to the inherent noise in gradient estimates or potentially poor initialization of A, updates might inadvertently lead to iterates $A^{(t)}$ that approach or even violate this constraint boundary. Such violations can cause numerical instability (e.g., 'log(0)' or 'log(negative number)') and large, uninformative gradients, hindering the convergence of the optimization process.

To address this, we propose a surrogate function $\hat{\mathcal{R}}_B[A]$ for the constraint $\mathcal{R}_B[A]$ that behaves more gracefully near and beyond the constraint boundary. Ideally, this surrogate should satisfy the following properties:

1. When the constraint $C(A, W^*) < B$ is satisfied (i.e., $\mathcal{R}_B[A] > 0$), the surrogate $\hat{\mathcal{R}}_B[A]$ should approximate the original constraint function $\mathcal{R}_B[A]$.
2. When the constraint $C(A, W^*) \geq B$ is violated (i.e., $\mathcal{R}_B[A] \leq 0$), the surrogate $\hat{\mathcal{R}}_B[A]$ should smoothly approach 0 from the positive side (0^+). This ensures that $\ln(\hat{\mathcal{R}}_B[A])$ remains defined and tends to $-\infty$, preserving the barrier effect without encountering numerical errors associated with non-positive arguments.
3. The surrogate function should be differentiable to allow for gradient-based optimization.

A suitable candidate that fulfills these requirements is a scaled and shifted softplus function. The softplus function is a smooth approximation of the rectifier function $\text{ReLU}(x) = \max(0, x)$. We define our surrogate constraint function $\hat{\mathcal{R}}_B[A]$ as:

$$\hat{\mathcal{R}}_B[A] = \beta \cdot \text{softplus}\left(\frac{\mathcal{R}_B[A]}{\beta}\right) = \beta \cdot \ln\left(1 + \exp\left(\frac{B - C(A, W^*)}{\beta}\right)\right) \tag{13}$$

where $\beta > 0$ is a temperature parameter that controls the smoothness of the approximation. It is worth noting that the softplus function is readily available in popular deep learning libraries such as PyTorch (as 'torch.nn.functional.softplus'). In our implementation, we can set $\beta = \mu^{(t)}$, the current barrier weight, allowing the sharpness of the surrogate to anneal along with the barrier itself. For simplicity in the main text, we denoted this as $\mu \ln(1 + \exp((B - C(A, W^*))/\mu))$, which corresponds to Equation 13 with $\beta = \mu$.

Let's verify the asymptotic properties of this surrogate $\hat{\mathcal{R}}_B[A]$ as defined in Equation 13, particularly focusing on its behavior as the original constraint $\mathcal{R}_B[A]$ varies:

Case 1: Constraint is well satisfied ($\mathcal{R}_B[A] \gg 0$) When $B - C(A, W^*) \gg 0$, then $\frac{\mathcal{R}_B[A]}{\beta} \gg 0$. In this regime, $\exp\left(\frac{\mathcal{R}_B[A]}{\beta}\right)$ is very large. So, $\ln\left(1 + \exp\left(\frac{\mathcal{R}_B[A]}{\beta}\right)\right) \approx \ln\left(\exp\left(\frac{\mathcal{R}_B[A]}{\beta}\right)\right) = \frac{\mathcal{R}_B[A]}{\beta}$. Therefore,

$$\hat{\mathcal{R}}_B[A] = \beta \cdot \text{softplus}\left(\frac{\mathcal{R}_B[A]}{\beta}\right) \approx \beta \cdot \frac{\mathcal{R}_B[A]}{\beta} = \mathcal{R}_B[A] = B - C(A, W^*). \tag{14}$$

This shows that when the constraint is comfortably met, the surrogate closely approximates the original constraint function.

Case 2: Constraint is violated or at the boundary ($\mathcal{R}_B[A] \ll 0$ or $\mathcal{R}_B[A] \approx 0$) When $B - C(A, W^*) \ll 0$ (constraint significantly violated), then $\frac{\mathcal{R}_B[A]}{\beta} \ll 0$. In this regime, $\exp\left(\frac{\mathcal{R}_B[A]}{\beta}\right) \approx 0$. So, $\ln\left(1 + \exp\left(\frac{\mathcal{R}_B[A]}{\beta}\right)\right) \approx \ln(1) = 0$. Therefore,

$$\hat{\mathcal{R}}_B[A] = \beta \cdot \text{softplus}\left(\frac{\mathcal{R}_B[A]}{\beta}\right) \approx \beta \cdot 0 = 0. \tag{15}$$

More precisely, as $\frac{\mathcal{R}_B[A]}{\beta} \to -\infty$, $\exp\left(\frac{\mathcal{R}_B[A]}{\beta}\right) \to 0^+$. Thus, $1 + \exp\left(\frac{\mathcal{R}_B[A]}{\beta}\right) \to 1^+$, and $\ln\left(1 + \exp\left(\frac{\mathcal{R}_B[A]}{\beta}\right)\right) \to 0^+$. Consequently, $\hat{\mathcal{R}}_B[A] \to 0^+$.

If $\mathcal{R}_B[A] = 0$ (at the boundary), then $\exp(0) = 1$, so

$$\hat{\mathcal{R}}_B[A] = \beta \ln(1 + \exp(0)) = \beta \ln(2). \tag{16}$$

As $\beta \to 0^+$ (which happens as $\mu^{(t)} \to 0^+$ during optimization), $\hat{\mathcal{R}}_B[A] \to 0^+$. This is consistent with the desired behavior where the barrier becomes increasingly sharp. The key is that for any fixed $\beta > 0$, if $\mathcal{R}_B[A]$ becomes sufficiently negative, $\hat{\mathcal{R}}_B[A]$ will approach 0 from the positive side.

This softplus-based surrogate $\hat{\mathcal{R}}_B[A]$ effectively smooths the hard constraint boundary, ensuring that the argument of the logarithm in the barrier term always remains positive. This allows SGD to navigate near the feasible region boundary more robustly, preventing numerical issues while still strongly penalizing constraint violations as $\mu^{(t)}$ (and thus β if $\beta = \mu^{(t)}$) decreases. This modification maintains the theoretical consistency with the original interior-point method while enhancing the stability of practical optimization with stochastic gradients.

B TABULAR RESULTS FOR THE MAIN PAPER

The results presented in the main paper are obtained by preserving the original activations. We use a block size of 32 for the MXFP format. Sections C appendix provide more experiments with quantized activations (MXFP4) and an additional set of experiments using 6.25 as max bit constraint (comparable to MXFP6 effective bits). Due to the supernet's nature, models momentarily take up to a maximum of 2x their original size during the search phase before the final compression during the rounding stage of the algorithm.

B.1 DETAILED EXPERIMENTAL SETUP

Table 1: Detailed Training Parameters. All experiments use Learning Rate = 0.1, Weight Decay = 0, Adam parameters (β_1=0.9, β_2=0.999, ϵ=1e-8), linear LR scheduler, 10 epochs, dataset = allenai/c4, and 128 samples for "fewshots" experiments, 256 samples for "zeroshot" experiments. All of the original model weights and parameters are frozen.

Model	Size	Max Bits	$\mu^{(0)}$	δ	$A^{l\,(0)}$	w_dtypes	Runtime
opt-125m	125M	4.5	0.50	0.2	[0.95, 0.05]	mxfp4, mxfp8	2.6m
opt-350m	350M	4.5	0.50	0.5	[0.95, 0.05]	mxfp4, mxfp8	6.9m
Qwen2.5-0.5B	500M	4.5	0.50	0.2	[0.95, 0.05]	mxfp4, mxfp8	9.3m
gemma-3-1b-it	1.0B	4.5	0.25	0.5	[0.95, 0.05]	mxfp4, mxfp8	18.2m
Llama-3.2-1B	1.0B	4.5	0.25	0.5	[0.95, 0.05]	mxfp4, mxfp8	20.5m
opt-1.3b	1.3B	4.5	0.25	0.5	[0.95, 0.05]	mxfp4, mxfp8	22.1m
Qwen2.5-1.5B	1.5B	4.5	0.50	0.2	[0.95, 0.05]	mxfp4, mxfp8	26.7m
gemma-2b	2.0B	4.5	0.25	0.5	[0.95, 0.05]	mxfp4, mxfp8	39.6m
Llama-3.2-3B	3.0B	4.5	0.25	0.5	[0.85, 0.15]	mxfp4, mxfp8	52.3m
Qwen2.5-3B	3.0B	4.5	0.25	0.5	[0.95, 0.05]	mxfp4, mxfp8	52.8m
gemma-3-4b-it	4.0B	4.5	0.50	0.2	[0.95, 0.05]	mxfp4, mxfp8	32.1m

B.2 DETAILED FEWSHOT RESULTS

Table 2: Results for **C4 Perplexity** (**lower is better**). Color indicates our method outperforms: MXFP4, MXFP6, or MXFP8 baseline.

Model	Size	MXFP4	MXFP6	MXFP8	Mixed 4.5 bits
opt-125m	125M	29.25	26.16	25.98	28.98
opt-350m	350M	24.79	22.20	21.96	22.05
Qwen2.5-0.5B	500M	23.60	20.56	20.05	21.09
gemma-3-1b-it	1.0B	42.06	37.24	35.78	35.48
Llama-3.2-1B	1.0B	19.13	16.51	16.11	16.21
opt-1.3b	1.3B	16.34	15.72	15.65	15.71
Qwen2.5-1.5B	1.5B	15.58	14.25	14.10	15.95
gemma-2b	2.0B	14.71	13.69	13.51	14.15
Llama-3.2-3B	3.0B	15.28	13.97	13.68	12.66
Qwen2.5-3B	3.0B	12.97	12.28	12.35	13.69
gemma-3-4b-it	4.0B	25.86	22.80	22.97	18.59

Table 3: Results for **C4 Accuracy** (**higher is better**). Color indicates our method outperforms: MXFP4, MXFP6, or MXFP8 baseline.

Model	Size	MXFP4	MXFP6	MXFP8	Mixed 4.5 bits
opt-125m	125M	37.9%	39.3%	39.4%	36.0%
opt-350m	350M	40.0%	41.4%	41.5%	41.5%
Qwen2.5-0.5B	500M	38.1%	39.9%	39.3%	40.7%
gemma-3-1b-it	1.0B	36.1%	37.8%	38.1%	36.5%
Llama-3.2-1B	1.0B	41.5%	43.6%	44.0%	42.4%
opt-1.3b	1.3B	44.4%	44.9%	45.0%	44.9%
Qwen2.5-1.5B	1.5B	43.0%	43.6%	43.7%	43.9%
gemma-2b	2.0B	44.9%	45.5%	46.1%	44.9%
Llama-3.2-3B	3.0B	44.6%	45.9%	46.2%	46.0%
Qwen2.5-3B	3.0B	44.4%	45.6%	45.8%	45.8%
gemma-3-4b-it	4.0B	42.1%	43.2%	43.4%	44.5%

B.3 DETAILED ZEROSHOT RESULTS

Table 4: Results for **LAMBADA** (**higher is better**). Color indicates our method outperforms: MXFP4, MXFP6, or MXFP8 baseline.

Model	Size	MXFP4	MXFP6	MXFP8	Mixed 4.5 bits
opt-125m	125M	37.6%	37.5%	37.1%	37.8%
opt-350m	350M	40.2%	45.8%	44.8%	44.9%
Qwen2.5-0.5B	500M	36.4%	49.3%	50.7%	50.5%
gemma-3-1b-it	1.0B	38.5%	43.1%	42.9%	45.0%
Llama-3.2-1B	1.0B	52.3%	61.1%	62.3%	59.0%
opt-1.3b	1.3B	57.4%	57.8%	57.8%	58.4%
Qwen2.5-1.5B	1.5B	59.7%	63.2%	62.0%	60.4%
gemma-2b	2.0B	58.9%	64.1%	65.8%	64.9%
Llama-3.2-3B	3.0B	68.0%	70.5%	70.4%	69.7%
Qwen2.5-3B	3.0B	65.7%	65.0%	67.4%	64.7%
gemma-3-4b-it	4.0B	56.4%	59.5%	59.6%	57.7%

Table 5: Results for **Wikitext Perplexity** (**lower is better**). Color indicates our method outperforms: MXFP4, MXFP6, or MXFP8 baseline.

Model	Size	MXFP4	MXFP6	MXFP8	Mixed 4.5 bits
opt-125m	125M	37.51	32.45	32.18	33.49
opt-350m	350M	29.70	26.05	25.65	25.67
Qwen2.5-0.5B	500M	22.07	18.29	17.83	18.00
gemma-3-1b-it	1.0B	36.69	30.83	29.56	27.71
Llama-3.2-1B	1.0B	14.25	11.89	11.67	12.53
opt-1.3b	1.3B	17.42	16.55	16.46	16.53
Qwen2.5-1.5B	1.5B	13.76	12.33	12.18	12.62
gemma-2b	2.0B	45.47	94.84	42.10	42.57
Llama-3.2-3B	3.0B	10.23	9.42	9.32	9.83
Qwen2.5-3B	3.0B	15.97	15.03	12.77	15.28
gemma-3-4b-it	4.0B	18.86	18.74	18.73	17.05

C MXFP4 ACTIVATIONS

C.1 EXPERIMENTAL SETUP

Table 6: Detailed Training Parameters. All experiments use Learning Rate = 0.1, Weight Decay = 0, Adam parameters (β_1=0.9, β_2=0.999, ϵ=1e-8), linear LR scheduler, 10 epochs, dataset = wikitext-2-raw, and 128 256 samples. All of the original model weights and parameters are frozen.

Model	Size	Max Bits	$\mu^{(0)}$	δ	$A^{l\,(0)}$	w_dtypes	Runtime
opt-125m	125M	4.5	0.50	0.5	[0.95, 0.05]	mxfp4, mxfp8	3.3m
opt-125m	125M	6.25	0.50	0.5	[0.8, 0.2]	mxfp4, mxfp8	3.3m
opt-350m	350M	4.5	0.50	0.5	[0.95, 0.05]	mxfp4, mxfp8	8.7m
opt-350m	350M	6.25	0.50	0.5	[0.8, 0.2]	mxfp4, mxfp8	8.7m
Qwen2.5-0.5B	500M	4.5	0.50	0.5	[0.95, 0.05]	mxfp4, mxfp8	11.5m
Qwen2.5-0.5B	500M	6.25	0.50	0.5	[0.8, 0.2]	mxfp4, mxfp8	11.5m
Llama-3.2-1B	1.0B	4.5	0.50	0.5	[0.95, 0.05]	mxfp4, mxfp8	23.1m
Llama-3.2-1B	1.0B	6.25	0.50	0.5	[0.8, 0.2]	mxfp4, mxfp8	23.1m
gemma-3-1b-pt	1.0B	4.5	0.50	0.5	[0.95, 0.05]	mxfp4, mxfp8	21.3m
gemma-3-1b-pt	1.0B	6.25	0.50	0.5	[0.8, 0.2]	mxfp4, mxfp8	21.3m
Qwen2.5-1.5B	1.5B	4.5	0.50	0.5	[0.95, 0.05]	mxfp4, mxfp8	31.0m
Qwen2.5-1.5B	1.5B	6.25	0.50	0.5	[0.8, 0.2]	mxfp4, mxfp8	31.0m
gemma-2-2b	2.0B	4.5	0.50	0.5	[0.95, 0.05]	mxfp4, mxfp8	49.4m
gemma-2-2b	2.0B	6.25	0.50	0.5	[0.8, 0.2]	mxfp4, mxfp8	49.5m
Llama-3.2-3B	3.0B	4.5	0.50	0.5	[0.95, 0.05]	mxfp4, mxfp8	1.0h
Llama-3.2-3B	3.0B	6.25	0.50	0.5	[0.8, 0.2]	mxfp4, mxfp8	1.0h
Qwen2.5-3B	3.0B	4.5	0.50	0.5	[0.95, 0.05]	mxfp4, mxfp8	59.3m
Qwen2.5-3B	3.0B	6.25	0.50	0.5	[0.8, 0.2]	mxfp4, mxfp8	59.3m

C.2 DETAILED FEWSHOTS RESULTS

Table 7: Results for **WikiText-2-raw Perplexity** (**lower is better**). Color indicates our method outperforms: MXFP4, MXFP6, or MXFP8 baseline.

Model	Size	MXFP4	MXFP6	MXFP8	Mixed 4.5	Mixed 6.25
opt-125m	125M	109.55	80.91	79.62	90.56	38.41
opt-350m	350M	68.39	55.07	53.74	58.96	28.95
Qwen2.5-0.5B	500M	33.23	21.28	20.13	23.55	12.58
Llama-3.2-1B	1.0B	50.35	29.09	27.28	32.12	20.52
gemma-3-1b-pt	1.0B	29.91	25.75	25.28	27.69	18.31
Qwen2.5-1.5B	1.5B	14.48	12.02	11.89	13.20	17.46
gemma-2-2b	2.0B	38.60	35.72	33.38	33.70	14.19
Llama-3.2-3B	3.0B	44.97	66.66	53.52	27.94	15.73
Qwen2.5-3B	3.0B	11.44	10.27	10.04	10.92	14.38

Table 8: Results for **WikiText-2-raw Accuracy** (**higher is better**). Color indicates our method outperforms: MXFP4, MXFP6, or MXFP8 baseline.

Model	Size	MXFP4	MXFP6	MXFP8	Mixed 4.5	Mixed 6.25
opt-125m	125M	25.2%	27.9%	28.1%	26.9%	32.8%
opt-350m	350M	28.9%	32.0%	32.2%	30.4%	36.0%
Qwen2.5-0.5B	500M	36.9%	41.8%	42.5%	40.6%	49.8%
Llama-3.2-1B	1.0B	34.7%	40.5%	41.4%	39.2%	40.5%
gemma-3-1b-pt	1.0B	40.1%	42.1%	42.1%	40.9%	41.9%
Qwen2.5-1.5B	1.5B	46.3%	48.6%	48.8%	47.3%	41.7%
gemma-2-2b	2.0B	39.1%	40.5%	41.1%	40.4%	44.9%
Llama-3.2-3B	3.0B	36.0%	32.7%	34.6%	40.8%	44.0%
Qwen2.5-3B	3.0B	49.1%	50.6%	51.0%	49.7%	42.3%

C.3 DETAILED ZEROSHOT RESULTS

Table 9: Results for **ARC-Challenge** (**higher is better**). Color indicates our method outperforms: MXFP4, MXFP6, or MXFP8 baseline.

Model	Size	MXFP4	MXFP6	MXFP8	Mixed 4.5	Mixed 6.25
opt-125m	125M	20.0%	19.6%	19.7%	19.2%	19.5%
opt-350m	350M	20.6%	20.1%	20.4%	21.1%	20.6%
Qwen2.5-0.5B	500M	27.0%	27.6%	28.9%	28.4%	28.5%
Llama-3.2-1B	1.0B	28.4%	31.9%	31.6%	29.4%	31.7%
gemma-3-1b-pt	1.0B	33.4%	34.6%	35.4%	34.0%	35.5%
Qwen2.5-1.5B	1.5B	40.4%	40.5%	42.2%	39.9%	41.2%
gemma-2-2b	2.0B	43.7%	45.6%	46.8%	44.5%	45.2%
Llama-3.2-3B	3.0B	41.3%	42.2%	41.7%	40.5%	42.1%
Qwen2.5-3B	3.0B	43.3%	44.0%	45.2%	44.1%	45.7%

Table 10: Results for **LAMBADA** (**higher is better**). Color indicates our method outperforms: MXFP4, MXFP6, or MXFP8 baseline.

Model	Size	MXFP4	MXFP6	MXFP8	Mixed 4.5	Mixed 6.25
opt-125m	125M	37.6%	37.5%	37.1%	37.3%	36.2%
opt-350m	350M	40.2%	45.8%	44.8%	42.0%	43.3%
Qwen2.5-0.5B	500M	36.4%	49.3%	50.7%	44.1%	47.6%
Llama-3.2-1B	1.0B	52.3%	61.1%	62.3%	54.1%	62.2%
gemma-3-1b-pt	1.0B	53.0%	56.1%	55.8%	53.9%	56.8%
Qwen2.5-1.5B	1.5B	59.7%	63.2%	62.0%	61.2%	62.3%
gemma-2-2b	2.0B	64.9%	69.5%	70.0%	66.5%	69.0%
Llama-3.2-3B	3.0B	68.0%	70.5%	70.4%	68.9%	69.9%
Qwen2.5-3B	3.0B	65.7%	65.0%	67.4%	68.4%	66.8%

D ADDITIONAL EXPERIMENTS

To demonstrate the robustness of our method across varying hardware constraints, we evaluated the performance of our Constrained Mixed Precision Search (CMPS) against uniform baselines across a continuous range of effective bit-widths.

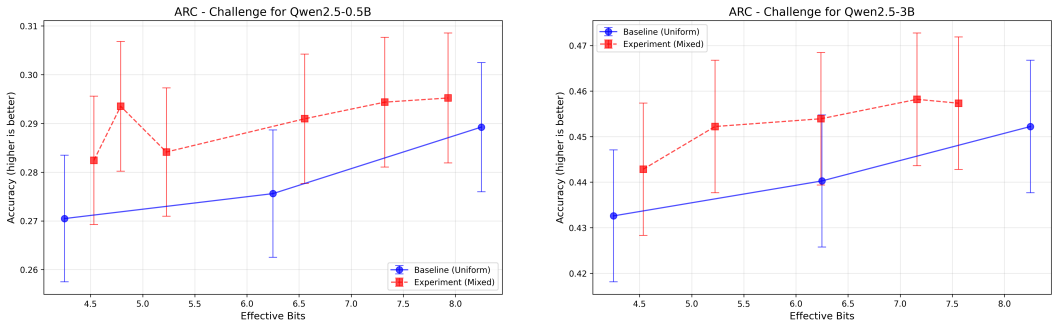

(a) Qwen2.5-0.5B (b) Qwen2.5-3B

Figure 6: **ARC-Challenge Accuracy vs. Effective Bits.** Comparison of our Mixed-Precision Search (Red) vs. Uniform Baselines (Blue). The mixed-precision approach consistently yields a superior Pareto frontier, achieving higher accuracy for the same effective bit budget across both model sizes.

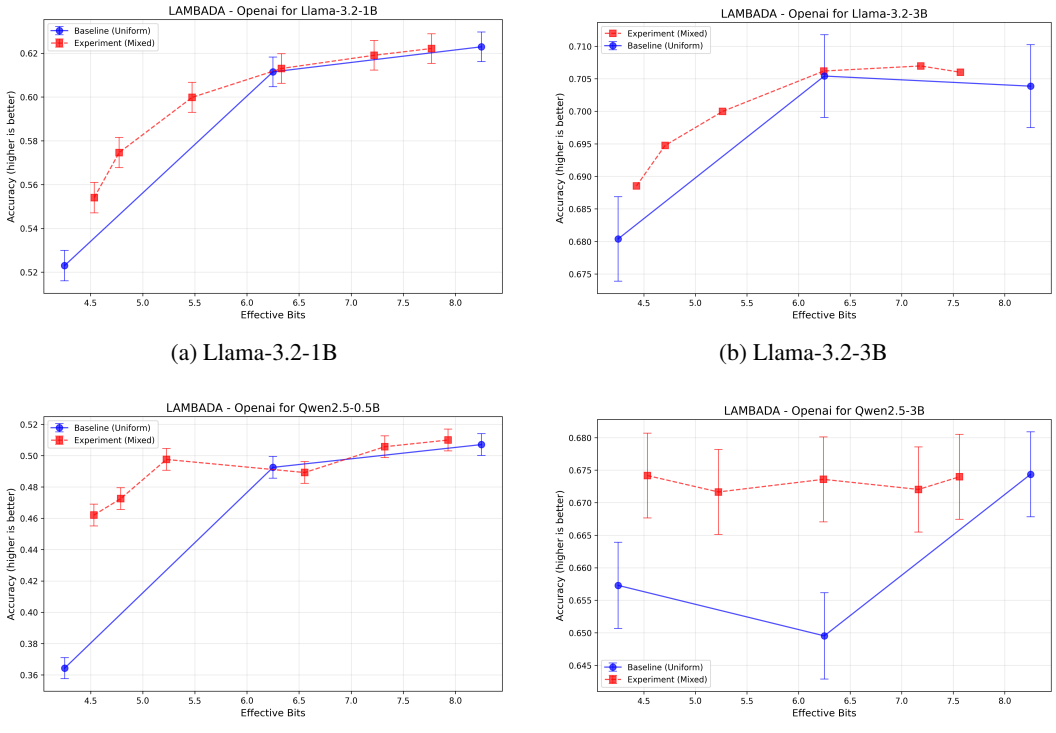

(a) Llama-3.2-1B (b) Llama-3.2-3B

(c) Qwen2.5-0.5B (d) Qwen2.5-3B

Figure 7: **LAMBADA (OpenAI) Accuracy vs. Effective Bits.** Our constrained optimization (Red dashed line) consistently outperforms the uniform quantization baseline (Blue solid line). Notably, our method frequently achieves the performance of higher-precision uniform models (e.g., 6-bit) while using significantly fewer bits (e.g., 4.5 bits).

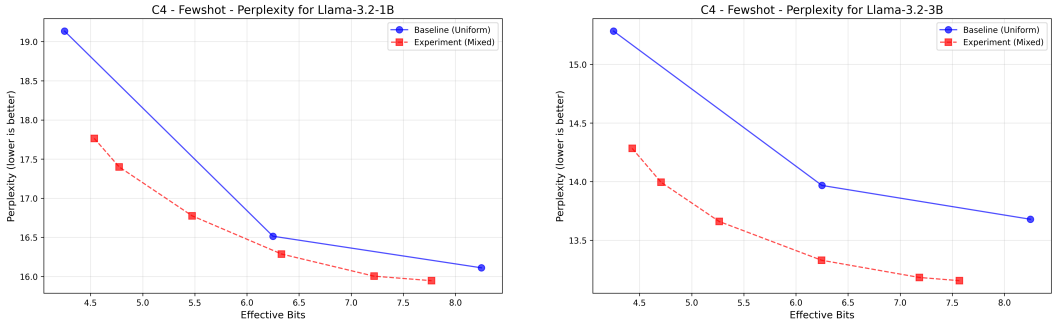

(a) Llama-3.2-1B (b) Llama-3.2-3B

Figure 8: **C4 Validation Perplexity vs. Effective Bits (Lower is Better).** The mixed-precision allocation provides a strictly better trade-off curve, achieving lower perplexity at every measured bit-width constraint compared to uniform MXFP quantization.

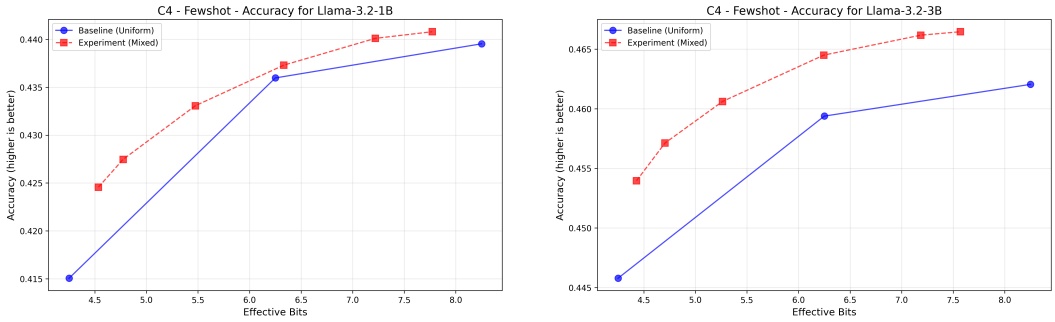

(a) Llama-3.2-1B (b) Llama-3.2-3B

Figure 9: **C4 Validation Accuracy vs. Effective Bits.** Similar to the perplexity results, the accuracy metric on the calibration domain (C4) shows that the learned allocation preserves model capability better than uniform baselines as the compression rate increases.